

Internal Residual Stresses in Sintered and Commercial Low Expansion $\text{Li}_2\text{O}-\text{Al}_2\text{O}_3-\text{SiO}_2$ Glass-Ceramics

Francisco C. Serbena,^{†,‡} Viviane Oliveira Soares,[§] Oscar Peitl,[§] Haroldo Pinto,[¶] Reginaldo Muccillo,^{||} and Edgar D. Zanotto[§]

[†]Department of Physics, State University of Ponta Grossa (UEPG), CEP 84030-900, Ponta Grossa, PR, Brazil

[§]Vitreous Materials Laboratory (LaMaV), Department of Materials Engineering (DEMA), Federal University of São Carlos (UFSCar), CEP 13565-905, São Carlos, SP, Brazil

[¶]Department of Materials, Aeronautic and Automotive Engineering, Engineering School of São Carlos (EESC), University of São Paulo (USP), CEP 13566-590, São Carlos, SP, Brazil

^{||}Center of Science and Technology of Materials, Energy and Nuclear Research Institute (IPEN), CEP 05508-900, São Paulo, SP, Brazil

We performed Synchrotron X-ray diffraction (XRD) analyses of internal residual stresses in monolithic samples of a newly developed $\text{Li}_2\text{O}-\text{Al}_2\text{O}_3-\text{SiO}_2$ (LAS) glass-ceramic produced by sintering and in a commercial LAS glass-ceramic, CERAN[®], produced by the traditional crystal nucleation and growth treatments. The elastic constants were measured by instrumented indentation and a pulse-echo technique. The thermal expansion coefficient of virgilite was determined by high temperature XRD and dilatometry. The *c*-axis contracts with the increasing temperature whereas the *a*-axis does not vary significantly. Microcracking of the microstructure affects the thermal expansion coefficients measured by dilatometry and thermal expansion hysteresis is observed for the sintered glass-ceramic as well as for CERAN[®]. The measured internal stress is quite low for both glass-ceramics and can be explained by theoretical modeling if the high volume fraction of the crystalline phase (virgilite) is considered. Using a modified Green model, the calculated critical (glass) island diameter for spontaneous cracking agreed with experimental observations. The experimental data collected also allowed the calculation of the critical crystal grain diameters for grain-boundary microcracking due to the anisotropy of thermal expansion of virgilite and for microcracking in the residual glass phase surrounding the virgilite particles. All these parameters are important for the successful microstructural design of sintered glass-ceramics.

I. Introduction

GLASS-CERAMICS are polycrystalline materials composed of one or more crystalline phases embedded in a residual glassy matrix obtained by controlled crystallization of certain glasses. The properties of glass-ceramics depend on their chemical composition and microstructure (volume fraction of crystalline and glassy phases, type, shape, and size of the crystals^{1,2}), and also on the magnitude and type of residual stresses that arise on cooling below the glass transition region. These residual stresses result from the superposition of macroscopic stresses caused by tem-

perature gradients across the sample cross section during the cooling process, the so-called thermal tempering stresses, with microscopic stresses due to the mismatch between the thermal and elastic properties of the crystalline and amorphous phases.³⁻⁶ The macroscopic stresses can be minimized or even eliminated by slow cooling or subsequent annealing,⁵ whereas the microscopic residual stresses are unavoidable and intrinsic to glass-ceramics owing to their heterogeneous multiphase nature, thus influencing crack nucleation and propagation in these materials.

Glass-ceramics of the $\text{Li}_2\text{O}-\text{Al}_2\text{O}_3-\text{SiO}_2$ (LAS) system are among the earliest developed and have achieved great industrial and commercial importance due to their extremely low thermal expansion coefficient.^{1,2} Their main crystalline phases are metastable solid solutions of the high-quartz or keatite structure, such as virgilite and β -spodumene. Both types of lithium aluminosilicates adopt the tridimensional structure of SiO_2 polymorphs, with AlO_4 tetrahedra linked through their corners to SiO_4 tetrahedra in an ordered or disordered way forming a tridimensional structure. Li^+ and Mg^{2+} ions occupy cavities in the structure and provide charge neutrality.² Owing to the occurrence of noncubic crystal structures in this system, the thermal expansion of those crystalline phases are highly anisotropic.^{2,7} This fact leads to a crystallographic dependence of the residual stresses for low crystalline volume fractions⁵ and also to intergranular stresses in highly crystalline glass-ceramics.

The most common method to produce glass-ceramics, such as the ultra-low-expansion LAS glass-ceramics CERAN[®], ZERO-DUR[®], KERALITE/PYROCERAM-III[®], CLEARCERAM[®]-Z, and similar brands, is by melting, vitrification, copious internal nucleation (induced by nucleating agents), and subsequent crystal growth in the interior of monolithic glass pieces. However, in principle, glass-ceramics can also be produced by sintering of glass powder compacts followed by controlled crystallization starting on the glass particle interfaces. In this process, surface defects on the glass particles act as nucleating sites and promote crystallization⁷; hence, there is no need to add catalyzers. However, it is not possible to produce dense glass-ceramics by this route if crystallization occurs before sintering.^{8,9}

The purpose of this work is therefore to assess the impact of the processing route on the residual stresses in LAS glass-ceramics. To this end, the residual stresses in the commercial glass-ceramic CERAN[®] produced by the traditional method are compared with those in an experimental glass-ceramic obtained by the powder sintering route. The role of crystalline volume fraction and thermal expansion anisotropy on residual stresses and microcracking is discussed.

D. J. Green—contributing editor

Manuscript No. 28346. Received July 17, 2010; approved September 28, 2010.

This work was financially supported by CNPq/Brazil-process no. 151917/2006-0, FAPESP/Brazil-contracts no. 07/08179-9 and 05/53241-9, CNPq and the Brazilian Synchrotron Light Laboratory/MCT research proposals XRD1-5824 and XRD1-6712.

[†]Author to whom correspondence should be addressed. e-mail: fserbena@uepg.br

II. Experimental Procedure

An LAS glass was obtained from analytical-grade raw materials. The mixture of precursor powders was melted in a platinum crucible at 1600°C for 3 h in an electrical furnace in air. The melt was quenched into water and the “frits” were crushed in a Fritsch Pulverisette (Idar-Oberstein, Germany) high-impact mill. The mean particle size after milling was about 4 μm.

A Netzsch DSC 404 (Selb, Germany) equipment was used for the determination of the characteristic temperatures of the glass powder in the heating curves using a heating rate of 10°C/min.

Small cylinders (diameter 10 mm, height 4 mm) were produced by isostatically pressing the glass powder at 200 MPa, which was then heated at 30°C/min in air to a temperature of 1000°C to obtain the sintered LAS glass–ceramic. The sample was then polished in a suspension of CeO₂. All the sintered glass–ceramic samples were produced at LaMaV, UFSCar, and are described in Table I. Two other glass samples were submitted to conventional heat treatments to produce a few isolated crystals (5 μm in diameter) at their surface (30 min at 900°C), and a crystallized surface layer over the glass (15 μm in thickness) (90 min at 900°C).

A stress-free reference sample was prepared from sintered LAS glass–ceramic by crushing in a Fritsch Pulverisette high impact mill, sieving, and annealing at 650°C for 15 min, followed by slow cooling to room temperature. The average particle size was 0.7 μm as measured by laser scattering using a Horiba LA930 device (Irvine, CA). Residual stress analyses were performed for as-sintered LAS glass–ceramic and for another sintered sample subjected to annealing at 650°C for 15 min and slowly cooled to room temperature to minimize possible macroscopic residual stresses, as well as for the two glass–ceramics samples with isolated crystals and a crystallized surface layer. For the sake of comparison, the residual stresses were also determined for a sample of commercial CERAN[®] (Shott, Mainz, Germany) glass–ceramic after annealing at 800°C for 15 min and slowly cooling to reduce possible macroscopic stresses.

The residual stresses were experimentally determined for the virgilitite crystals using Rietveld refinement. The diffractograms of all samples given in Table I were measured in the θ – 2θ geometry at room temperature using the XPD beamline of the Brazilian National Synchrotron Light Laboratory (LNLS) and a (002) highly oriented pyrolytic graphite analyzer. The wavelength was set to 1.550274(4) Å, calibrated against a LaB₆ standard NIST-660a. The 2θ -range was scanned from 10° to 90° or 120° and the step size amounted to 0.01° or 0.02° in the 2θ -scale. The samples were rotated during the measurements to minimize the possible effect of texture or poor grain statistics. The lattice parameters of

the glass-ceramic samples and the stress-free reference were refined based on their complete diffractograms using the GSAS and the EXPGUI package.^{10,11} The lattice strains of the crystalline phase were evaluated for each glass–ceramic sample assuming the powdered LAS sample as a stress-free reference.

As the virgilitite unit cell is hexagonal, its average strain, $\bar{\epsilon}_v$, was calculated from the a and c lattice parameters by:

$$\bar{\epsilon}_v = \frac{2}{3} \frac{\Delta a}{a} + \frac{1}{3} \frac{\Delta c}{c} = \frac{2}{3} \epsilon_a + \frac{1}{3} \epsilon_c \quad (1)$$

where Δa and Δc are the differences between the lattice parameters of the strained and the stress-free samples and $\epsilon_a = \Delta a/a$ and $\epsilon_c = \Delta c/c$ are the strains along the a and c crystal directions.

The average stresses of virgilitite, $\bar{\sigma}_v$, in the sintered LAS and commercial CERAN[®] samples were then calculated using Hooke’s law and assuming a hydrostatic triaxial stress state of the crystals:

$$\bar{\sigma}_v = \frac{E_v}{(1 - 2\nu_v)} \bar{\epsilon}_v \quad (2)$$

where E_v is the elastic modulus and ν_v is Poisson’s ratio of virgilitite. For the heat-treated glass–ceramics with small surface crystals or a top crystallized layer, the average stresses of virgilitite were calculated from Hooke’s law using Eq. (3)¹²:

$$\bar{\sigma}_v = -\frac{E_v}{2\nu_v} \bar{\epsilon}_v \quad (3)$$

where it is assumed that the virgilitite crystals are subjected to a biaxial stress state with rotational symmetry and the stress component normal to the surface is negligible.

In order to enable a theoretical estimation of the residual stresses, the crystalline volume fraction, the average linear thermal expansion and its crystallographic dependence, as well as the elastic constants were measured for the glass and the crystalline phase.

The crystallized volume fraction was determined by X-ray diffraction (XRD). Alumina powder was mixed to the powdered samples of both, the sintered LAS and the CERAN[®], in a 1 to 1 proportion by weight. The diffractograms were recorded using CuK α radiation using a Rigaku diffractometer model Ultima IV (Tokyo, Japan). They were measured in θ – θ geometry and the 2θ -range was scanned from 10° to 120° with a step size of 0.02° in the 2θ -scale. The volume fractions of virgilitite and alumina were determined by Rietveld refinement of the XRD patterns, where the amorphous contribution was considered as part of the background. Using the known amount of alumina added to the powdered glass–ceramics and its estimated fraction obtained by the Rietveld refinements, a simple rule of mixture allowed for the calculation of the volume fractions of virgilitite and glass in the sintered LAS and the CERAN[®].

The thermal expansion coefficients of virgilitite are not documented in the literature. Hence, we estimated them using two different approaches: high-temperature XRD and dilatometry.

Its crystallographic dependence was determined by high-temperature XRD in θ – θ geometry using a Bruker-AXS diffractometer model D8 Advance (Karlsruhe, Germany), equipped with a Braun position sensitive detector (Graz, Austria) and an Anton Paar HTK1400 (Graz, Austria) heating stage, and a sintered LAS powdered sample. The diffractograms were recorded for the 2θ -range of 5°–80° in 0.035° steps at 20°, 200°, 400°, and 600°C using CuK α radiation. Rietveld refinement of the diffractograms recorded at each temperature was carried out using the GSAS and the EXPGUI package^{10,11} in order to determine the lattice parameter variations with temperature.

The average thermal expansion of virgilitite was evaluated by dilatometry of the glass α_g and the sintered LAS glass–ceramic α_{gc} using a Netzsch DIL 402 PC dilatometer and a heating rate of 5 K/min in air. The glass and sintered glass–ceramic samples of 3 mm × 2 mm × 40 mm were prepared by cutting and pol-

Table I. Samples and Heat Treatment Details Used in this Work

Sample	Heat treatment
Powder	Sintered at 1000°C with 30°C/min, cooled to RT at 15°C/min, powdered in a mortar, sieved in a 22 μm mesh, annealed at 650°C for 15 min, and cooled at 1°C/min to RT
Sintered	Sintered at 1000°C with 30°C/min, cooled to RT at 15°C/min
Sintered and annealed	Sintered at 1000°C with 30°C/min, annealed at 650°C for 15 min, cooled to RT at 1°C/min
Glass with isolated 5 μm crystals at the surface	Heat treated at 900°C for 30 min
Glass with crystallized surface	Heat treated at 900°C for 90 min
CERAN [®]	Annealed at 800°C for 15 min and slowly cooled

ishing to obtain parallel faces. The average thermal expansion of virgillite, α_v , was calculated from its dilatometric curve constructed by applying a rule of mixture for each temperature:

$$\alpha_v = \frac{\alpha_{gc} - V_f^G \alpha_G}{V_f^V} \quad (4)$$

where V_f^G and V_f^V are the volume fractions of the residual glass and virgillite, respectively, determined by XRD.

The influence of thermal shock on the thermal expansion behavior of the sintered LAS glass-ceramic and CERAN[®] was also investigated by dilatometry using a Netzsch DIL 402 PC dilatometer at 1°C/min. A single sample of each material was subjected to thermal shock cycles before the dilatometry measurements. Each thermal shock cycle consisted of heating the sample up to 600°C and quenching it into a bath of water and ice at 0°C for five times. After each thermal shock cycle, the thermal expansion was measured on heating up to a maximum temperature of 400°C and cooling down to room temperature using a heating and cooling rates of 5°C/min.

Elastic modulus (E) and hardness (H) were measured by instrumented nanoindentation (Nanoindenter XP MTS, Eden Prairie, MN) using the Oliver and Pharr method¹³ with a Berkovich diamond indenter. The maximum load was 400 mN. Each data point was calculated from the average of at least nine indentations. The elastic modulus and Poisson's ratio were measured using a pulse-echo technique.

III. Results

Figure 1 shows the Rietveld and Le Bail plots for the different samples studied in this work. Rietveld refinement was performed for all samples given in Table I. The chemical composition for virgillite was assumed as $\text{LiAlSi}_2\text{O}_6$. The Rietveld method does not yield a reasonable fit for the heat-treated glass-ceramics having individual surface crystals or with a top crystallized sur-

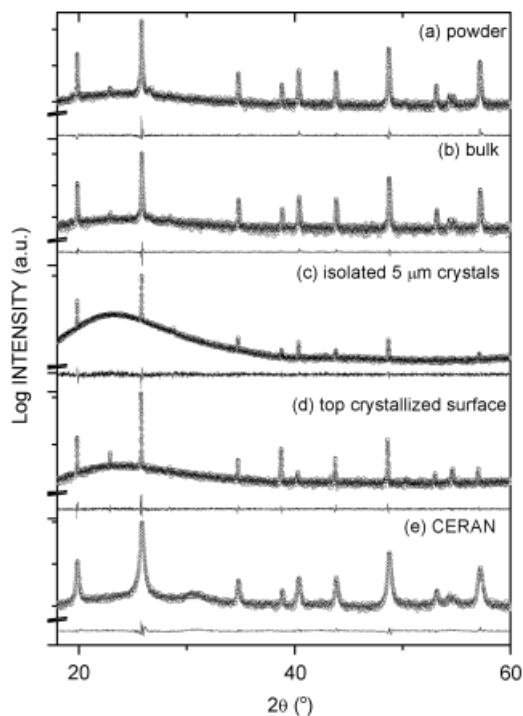


Fig. 1. Plots for the (a) powder, (b) sintered, (c) glass with some 5 μm crystals at the surface, (d) glass with a top crystallized layer, and (e) CERAN[®]. The observed intensity is represented by full circles, the calculated intensities and the difference curves are in black. Rietveld refinement was performed for samples (a), (b), and (e). The Le Bail method was used for samples (c) and (d).

face. A good fit was only possible using the Le Bail method. A possible explanation is that due to the low number of crystals on the surface of these samples, the peak intensities are affected by poor grain statistics.

A few peaks of small intensity that do not belong to virgillite were observed in all diffractograms. No exact match with any compound was achieved even after extensive search in the JCPDS-ICDD database. We attributed them to some unknown solid solution of Li-Al-Si-O formed during sintering. We included these peaks in the refinement as β -spodumene and used the Le Bail method for its fitting.

The refined lattice parameters a and c of virgillite in the different samples are shown in Table II. The strains are compressive and highly anisotropic in the sintered and CERAN[®] samples: the component along the c direction is more than one order of magnitude larger than along the basal plane. On the other hand, the virgillite crystals have tensile strains in both crystallographic directions in the heat-treated glass-ceramics with isolated crystals and with a top crystallized surface.

The average hydrostatic residual stress of virgillite in the sintered LAS glass-ceramic (annealed and nonannealed) and the commercial CERAN[®], determined using Eq. (2), are low, $-34(9)$ and $-87(5)$ MPa, respectively. The numbers in brackets are the standard deviations with one significant digit and they are the uncertainty in the last significant digit. On the other hand, although the virgillite crystals are expected to develop in all LAS glass-ceramics compressive stresses owing to its smaller (negative) coefficient of thermal expansion, tensile strains were determined for virgillite in the heat-treated glass-ceramics with isolated crystals or a top crystallized layer. This confirms the assumption of a biaxial stress state with rotational symmetry for these samples, because the Rietveld method provided the strain along the sample direction (surface normal) perpendicular to the existing in-plane compressive stresses. According to Hooke's Law, an elongation occurs along the surface normal in this case. Thus, the residual stresses for the sample with small isolated surface crystals and the one with a top crystallized layer according to Eq. (3) are highly compressive: $-250(4)$ and $-381(5)$ MPa, respectively.

The volume fraction of virgillite estimated from the Rietveld refinements of a 1-1 mixture by weight of alumina and sintered glass-ceramic powder was 84.1(3)% for the sintered glass-ceramic and 67.4(2)% for CERAN[®], indicating a considerable amount of crystalline phase. In the sintered glass-ceramic, a volume fraction of 4.6(2)% of an extra crystalline phase attributed to β -spodumene was also determined.

Figures 2(a) and (b) show the variation of the refined lattice parameters of virgillite with temperature. The thermal expansion coefficients were $-0.2(2) \times 10^{-6}$ and $-3.4(3) \times 10^{-6} \text{ } ^\circ\text{C}^{-1}$ along the crystal directions a and c , respectively. The average thermal expansion coefficient of virgillite was then estimated as:

$$\bar{\alpha}_v = \frac{2}{3}\alpha_a + \frac{1}{3}\alpha_c \quad (5)$$

and yielded an average thermal expansion coefficient of $-1.3(2) \times 10^{-6} \text{ } ^\circ\text{C}^{-1}$.

Figure 3 shows the linear thermal expansion coefficient of the parent glass and the sintered glass-ceramic with 89% crystallized volume fraction, measured by dilatometry, and the calculated thermal expansion curve of virgillite according to Eq. (4). In this case, we have added the small volume fraction of β -spodumene to the total volume fraction of virgillite. The sintered LAS glass-ceramic has a very low thermal expansion coefficient, $-2.1(3) \times 10^{-8} \text{ } ^\circ\text{C}^{-1}$. The thermal expansion coefficient of the parent glass was $4.550(2) \times 10^{-6} \text{ } ^\circ\text{C}^{-1}$ and the estimated linear thermal expansion coefficient of virgillite was $-0.557(3) \times 10^{-6} \text{ } ^\circ\text{C}^{-1}$ in the range of 50°–500°C, which is about 60% lower than the value measured by XRD. The difference observed between the thermal expansion of virgillite measured by XRD and dilatometry can be attributed to the change in the thermal expansion of the glass after crystallization (the chemical composition of the parent glass changes during crystallization, affecting its

Table II. Virgilite Lattice Parameters Obtained from Rietveld Refinement and Experimental Strains and Stresses Calculated According to Eqs. (1)–(3)

Sample	a (Å)	c (Å)	ε_a (%)	ε_c (%)	$\bar{\varepsilon}_v$ (%)	$\bar{\sigma}_v$ (MPa)
Powder	5.17893 (3)	5.45189 (4)	—	—	—	—
Sintered	5.17877 (3)	5.44917 (5)	−0.003 (1)	−0.050 (2)	−0.019 (5)	−34 (9)
Sintered/annealed	5.17875 (2)	5.44929 (4)	−0.003 (1)	−0.048 (1)	−0.018 (4)	−33 (6)
Glass/5 μm crystals	5.18918 (8)	5.4576 (1)	0.198 (2)	0.105 (3)	0.167 (3)	−250 (4)
Glass/crystallized surface	5.1935 (2)	5.46716 (9)	0.281 (4)	0.280 (2)	0.281 (4)	−381 (5)
CERAN [®] /annealed	5.1789 (1)	5.444 (2)	−0.001 (2)	−0.145 (4)	−0.049 (3)	−87 (5)

E_p and ν_p were 82.5 GPa and 0.27, respectively.

thermal expansion), to the microcracking of the microstructure (as discussed below), and to uncertainties in the estimative of the crystalline volume.

The sintered glass–ceramic and the commercial CERAN[®] revealed thermal expansion hysteresis (measured at 100°C) when tested in the temperature range of 20°–400°C in the dilatometer, as shown in Fig. 4(a) after the thermal shock cycles. This hysteresis increases after submitting the samples to subsequent thermal shock cycles as observed in Fig. 4(b), where, in each cycle, the sample was heated at 600°C and quenched at 0°C for five times. The increase in the hysteresis loops is more pronounced for the CERAN[®], whereas the data for the sintered glass–ceramic are somewhat scattered.

The sintered LAS glass–ceramics (not submitted to thermal shock) revealed an extensive number of cracks when examined by optical microscopy or SEM. Figure 5(a) shows that the larger residual glass islands exhibit extensive crack formation. In addition, a network of thin cracks is observed in Fig. 5(b) when the

sample is thinned down by careful polishing to a thickness of approximately 20 μm and examined under transmitted light. The microstructure of the sintered glass–ceramics consists of large glass particles and smaller rounded virgilite crystals embedded in residual glass as observed in Fig. 5(c). Owing to the high crystallized volume fraction, the crystals are in contact with their neighbors. When a fractured surface is examined under an SEM, very small features, which could be related to cracks or pores produced during sintering, are observed in the nm range as displayed in Fig. 5(d). However, cracks do not occur in CERAN[®] samples and in the heat-treated glass–ceramics with isolated crystals at the surface as revealed by Figs. 6(a) and (b). The estimated average crystal diameters are ~ 800 nm for the sintered LAS glass–ceramic and 60 nm for CERAN[®].

Figure 7 shows typical loading and unloading curves of the nanoindentation experiments for the samples tested. No pop-in is observed and all the curves are similar. Figures 8(a) and (b) show the hardness and elastic modulus variation as a function of contact depth. Their values at maximum contact depth are displayed in Table III. Also included are the values of elastic modulus and Poisson's ratio measured by the pulse-echo technique. The elastic modulus of virgilite calculated from the values of the glass and the sintered glass–ceramic by a rule of mixture was used for comparison with the elastic modulus from the LAS glass with a top crystallized surface measured by nanoindentation. In the rule of mixture, the properties of the residual glass and of β -spodumene were considered.

Their volume fractions were measured by XRD previously. For determination of E and ν of β -spodumene, a sample with 75% volume fraction of crystallized β -spodumene was prepared by sintering (volume fraction determined by XRD) for measurements using the pulse-echo technique. The E and ν of β -spodumene determined by the rule of mixture were 76.2 GPa and 0.26, respectively.

The glass and the sintered glass–ceramic have the lowest hardness. The hardness of the crystallized surface layer was approximately 10% higher, whereas CERAN[®] is the hardest material.

The elastic modulus showed little variation between the different samples. Only the commercial CERAN[®] exhibited a 10% higher elastic modulus. The elastic modulus of the glass obtained

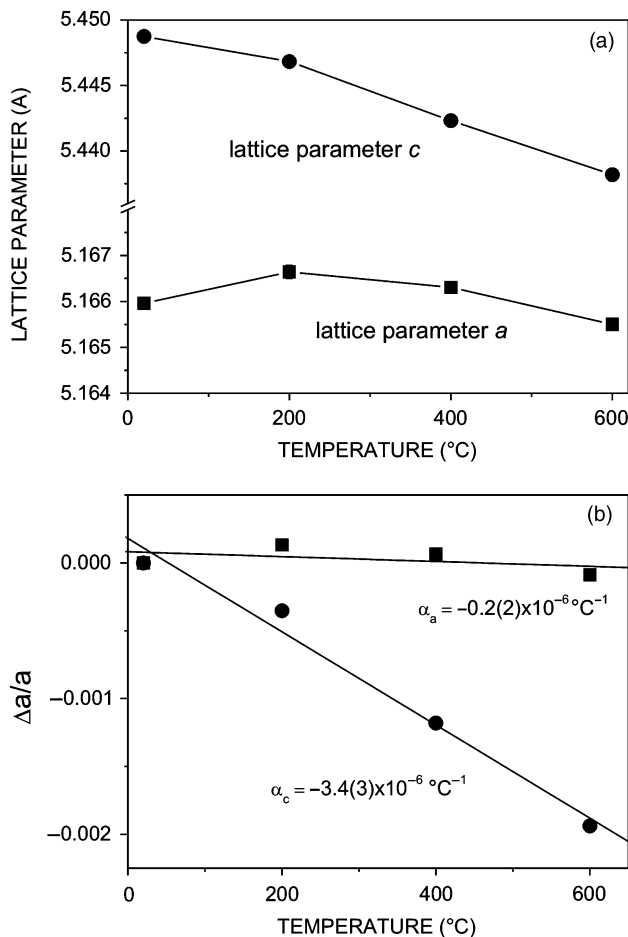


Fig. 2. (a) Variation of the lattice parameters a and c of the hexagonal unit cell of virgilite with temperature as measured by high-temperature X-ray diffraction and (b) their relative linear thermal expansion variation with temperature.

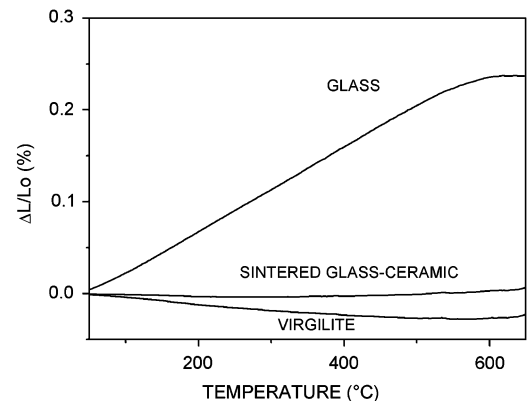


Fig. 3. Linear thermal expansion curves of glass and sintered glass–ceramic. The thermal expansion of virgilite was calculated using Eq. (4).

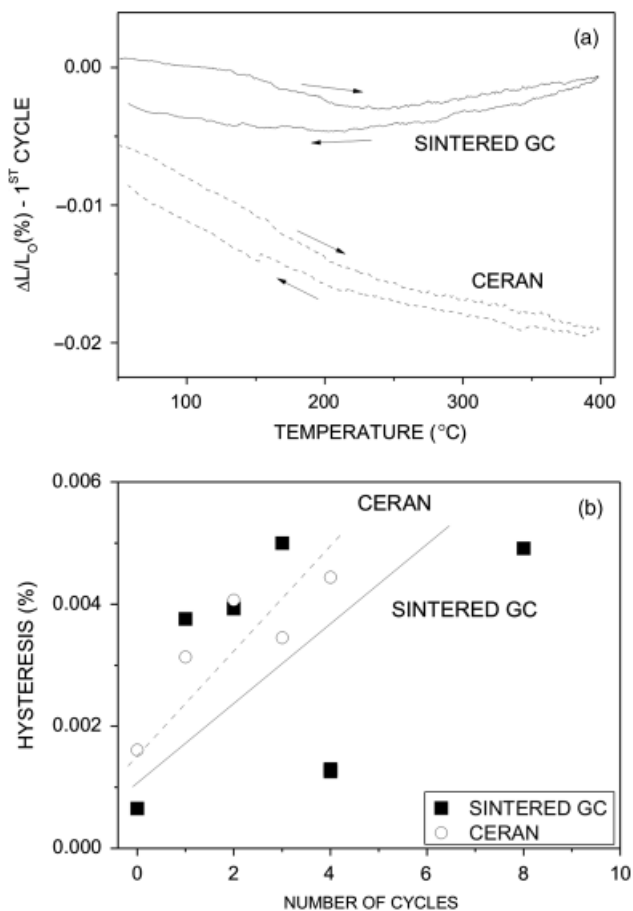


Fig. 4. (a) Thermal expansion hysteresis of the sintered glass-ceramic and CERAN[®] after the first thermal-shock cycle of heating-quenching from room temperature to 600°C and quenching at 0°C and (b) accumulated hysteresis as a function of number of thermal cycles measured at 100°C. The lines are a guide to the eyes only.

by instrumented indentation is in agreement with that measured by the pulse-echo technique. The elastic modulus of the sintered glass-ceramic and the crystallized surface measured by nanoindentation are about 10% lower than that of the glass sample.

Since nanoindentation measures the mechanical properties at shallow depths, the hardness and elastic modulus of the glass with a crystallized surface layer should be close to those of virgilitite. It is established that if the contact depth is $<1/10$ of the film thickness, the measured hardness and elastic modulus are those of the film and are not affected by the substrate. Because the crystallized layer thickness is approximately 15 μm , the hardness and elastic modulus of this sample correspond to those of virgilitite. However, the highest hardness and elastic modulus were encountered for CERAN[®] and this difference possibly reflects the different chemical composition of these two types of glass-ceramics.

IV. Discussion

A model to predict residual stresses in glass-ceramics having low volume fraction of a crystalline phase dispersed in a glass matrix was proposed by Selsing.¹⁴ This model was successfully tested in Mastelaro and colleagues.³⁻⁶ The Selsing model assumes that the precipitates are spherical and isotropic and that the stress fields around the precipitates do not overlap. According to their model, the hydrostatic pressure P inside each precipitate is:

$$P = \frac{\Delta\alpha\Delta T}{\frac{1 + \nu_m}{2E_m} + \frac{1 - 2\nu_p}{E_p}} \quad (6)$$

where E is the elastic modulus, ν is Poisson's ratio, the subscripts m and p refer to matrix and particle, $\Delta\alpha$ is the linear thermal expansion difference between the precipitate and the glass, and ΔT is assumed as the difference between T_g (when the glass stops to flow on cooling) and room temperature. For the LAS glass (matrix), we assume the experimental values $E_m = E_g = 76$ GPa, $\nu_m = \nu_g = 0.21$, and $\alpha_g = 4.6 \times 10^{-6} \text{ } ^\circ\text{C}^{-1}$. For the virgilitite precipitates, we assume $E_p = E_v = 82.5$ GPa, $\nu_p = \nu_v = 0.27$, and the average $\bar{\alpha}_v = -1.3 \times 10^{-6} \text{ } ^\circ\text{C}^{-1}$. Substituting these values in Eq. (6) and using $\Delta T = 650^\circ - 20^\circ\text{C} = 630^\circ\text{C}$, one obtains compressive stresses of -275 MPa in the virgilitite crystals.

Although Selsing's equation is valid for an isolated precipitate completely embedded in the matrix and not at the surface, where image stresses play an important role, it will be used to estimate the stresses in the case of the heat-treated LAS glass with 5 μm diameter individual crystals on the surface. The experimental strains lead to a calculated stress of $-250(4)$ MPa, i.e. 10% lower than the predicted value.

For the LAS glass with a 15 μm crystallized layer, the experimental stress is $-381(5)$ MPa. In this particular case of a film on a surface, thermal stresses arise during cooling if the thermal expansion coefficients of the film and substrate are different. For the case of a thin film, where the film thickness is much smaller than the substrate thickness, the thermal residual stress in the film σ_f is given by the following equation¹⁵:

$$\sigma_f = \frac{E_v \Delta\alpha \Delta T}{(1 - \nu_v)} \quad (7)$$

where E_v and ν_v represent the elastic modulus and Poisson's ratio of the virgilitite, respectively.

A residual stress of -420 MPa is predicted for the virgilitite layer. This is only 10% larger than the stress value determined by XRD. The main reason for this difference is most likely the thermal and/or elastic anisotropy of virgilitite.

The crystalline volume fraction of the sintered LAS glass-ceramic and CERAN[®] samples is estimated as 89% (virgilitite plus β -spodumene) and 67%, respectively. Selsing's model predicts that the stresses are constant and hydrostatic inside the precipitates and decay as $1/r^3$ in the matrix. In the sintered LAS glass-ceramic and the commercial CERAN[®], the residual glass phase can be treated as the "precipitate" surrounded by a matrix of virgilitite and residual glass. In this case, the stresses in the glass are constant and hydrostatic and the residual stresses in the matrix decays as $1/r^3$ from the precipitate. Therefore, the experimentally determined stresses represent an average value of this gradient and the stress superposition of other grains. Hsueh and Becher¹⁶ calculated the elastic isotropic solutions for residual stresses in spherical particles taking into account the volume fraction. Their proposal for the stress σ_p inside the precipitate is:

$$\sigma_p = \sigma_G = \frac{\Delta\alpha\Delta T}{\frac{1}{3K_p} + \frac{1}{4(1-f)G_m} + \frac{1}{3(1-f)K_m}} \quad (8)$$

where σ_G is the stress inside the glass precipitate within the sintered LAS and CERAN[®] samples, G is the shear modulus, K is the bulk modulus, and f is the volume fraction of inclusions. The subscripts m and p refer to matrix (virgilitite) and particle (glass islands), respectively. If $f=0$, the equation reduces to Selsing's equation. Assuming $G_p = G_G = 31.4$ GPa, $G_m = G_v = 32.5$ GPa, $K_p = K_G = 43.7$ GPa, $K_m = K_v = 59.8$ GPa, and $f=0.11$, a tensile stress $\sigma_G = \sigma_p$ of 219 MPa is calculated for the glass, where the subscripts G and V refer to glass and virgilitite, respectively. The average stress in the virgilitite $\bar{\sigma}_v$ can be obtained from the stress of the glass precipitates σ_G (Eq. (8)) using the following equilibrium condition:

$$f\sigma_G + (1-f)\bar{\sigma}_v = 0 \quad (9)$$

Equation (9) yields $\bar{\sigma}_v = -28$ MPa for the virgilitite crystals in the sintered LAS glass-ceramic, which is close to $-34(9)$ MPa

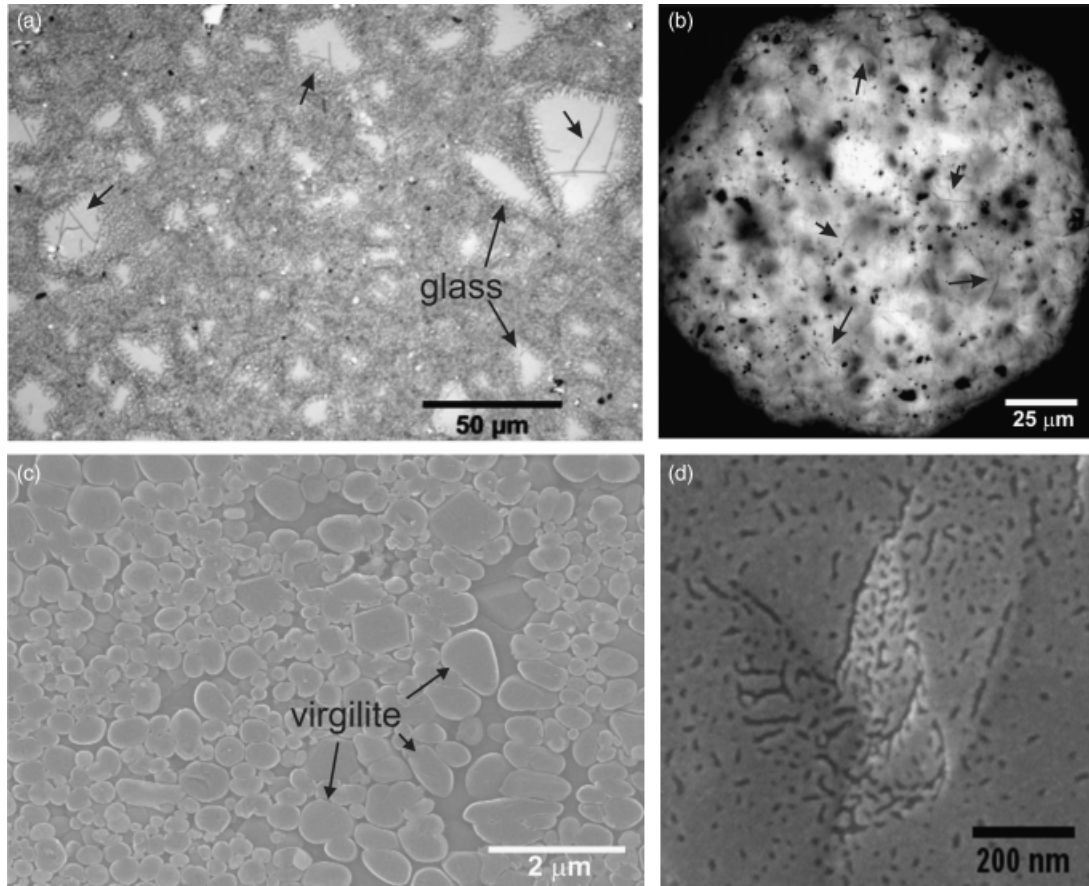


Fig. 5. Microcracks visible by optical microscopy of (a) a sample etched in diluted HF solution, (b) a sample with 20 μm thickness, and SEM of (c) a sample etched in diluted HF solution, (d) fracture surface of the sintered glass–ceramic. The HF solution removed the glass between the virgillite grains in (c). Cracks are indicated by arrows.

determined experimentally. Similar calculations reveal a tensile stress of 170 MPa in the glass matrix and an average compressive stress of -84 MPa for the virgillite precipitates in the CERAN[®] sample. This value is in agreement with the residual stress of $-87(5)$ MPa provided by the XRD measurements.

One point to mention is the stress state in different samples. The stress state is determined by the microstructure length scale and the material properties. In the specific case of a precipitate embedded in a matrix near the surface, Mindling and Cheng,¹⁷ assuming only elastic deformation, showed that the stress state inside a precipitate depends on the ratio between the location of the precipitate with respect to the surface (i.e., radius depth) and the radius of the precipitate. If this ratio is >2.5 , there should be no difference between the stresses inside a precipitate located near the surface and those in a precipitate embedded in an infinite matrix (i.e., in the bulk of the sample). Therefore, if the precipitate diameter is 100 nm, at a depth of 250 nm, its stress state can be considered as triaxial and Selsing's model is valid. However, for a larger precipitate with a diameter of a few hundred μm , a biaxial stress state might be more appropriate near the surface.

The penetration depth τ for the Synchrotron XRD experiments performed in this work can be calculated as $\tau = (1/2\mu)\sin\theta$, where μ is the linear attenuation coefficient of the glass–ceramic.¹⁸ Assuming the virgillite stoichiometry as $\text{LiAlSi}_2\text{O}_6$, its density as 2.46 g/cm^3 and $2\theta = 80^\circ$ for experiments in θ - 2θ configuration, the penetration depth is about 40 μm for $\lambda = 1.541$ Å. The average virgillite crystal size is approximately 800 nm. Therefore, we expect only the few crystals near the surface, up to a depth of ~ 1.2 μm , to be in a biaxial stress state. For deeper crystals, the assumption of triaxial stress state is reasonable. This assumption has been verified experimentally and theoretically. Levin *et al.*¹⁹ measured the residual stresses by the $\sin^2\psi$ technique in nanocrystals of SiC dispersed in an alumina matrix. The macrostresses were zero at

the surface, but the microstresses in the precipitates due to thermal and elastic mismatches between the precipitate and the matrix developed a triaxial state. Peitl *et al.*²⁰ calculated numerically the residual stresses in the matrix around a hemispherical precipitate at the surface. They found the stress state to be in plane stress condition near the surface. For the heat-treated glass–ceramics with a crystallized surface layer and individual crystals on the surface, the stress state is determined by the microstructure length scale: the thickness of the crystallized layer (15 μm) and the diameter of the individual crystals (5 μm), respectively. Therefore, the assumption of a biaxial stress state is justified.

The residual stresses determined for the as-sintered and the sintered and annealed glass–ceramics by XRD are very similar as displayed in Table II, indicating that there are no residual macrostresses in the as-sintered sample.

The temporarily stresses induced during the thermal shock experiments can be calculated. A simple estimate of the maximum thermal stress on quenching at the surface σ_t is given by the following equation²¹:

$$\sigma_t = \frac{E_{gc}\alpha_{gc}\Delta T}{(1 - \nu_{gc})} \quad (10)$$

where E_{gc} and ν_{gc} are the elastic modulus and Poisson's ratio of the glass–ceramic and it is assumed that the sample surface attains instantaneously the temperature of the quenching medium and there is no heat transfer from the interior to the surface of the sample. Assuming $E_{gc} = 82.5$ GPa, $\nu_{gc} = 0.26$, $\alpha_{gc} = 2.1 \times 10^{-8}$ $^\circ\text{C}^{-1}$, and $\Delta T = 630^\circ\text{C}$, a thermal stress of only 1.5 MPa is calculated.

Microcracking of the larger glass precipitates was observed in the sintered samples. The thermal residual stress of the glass

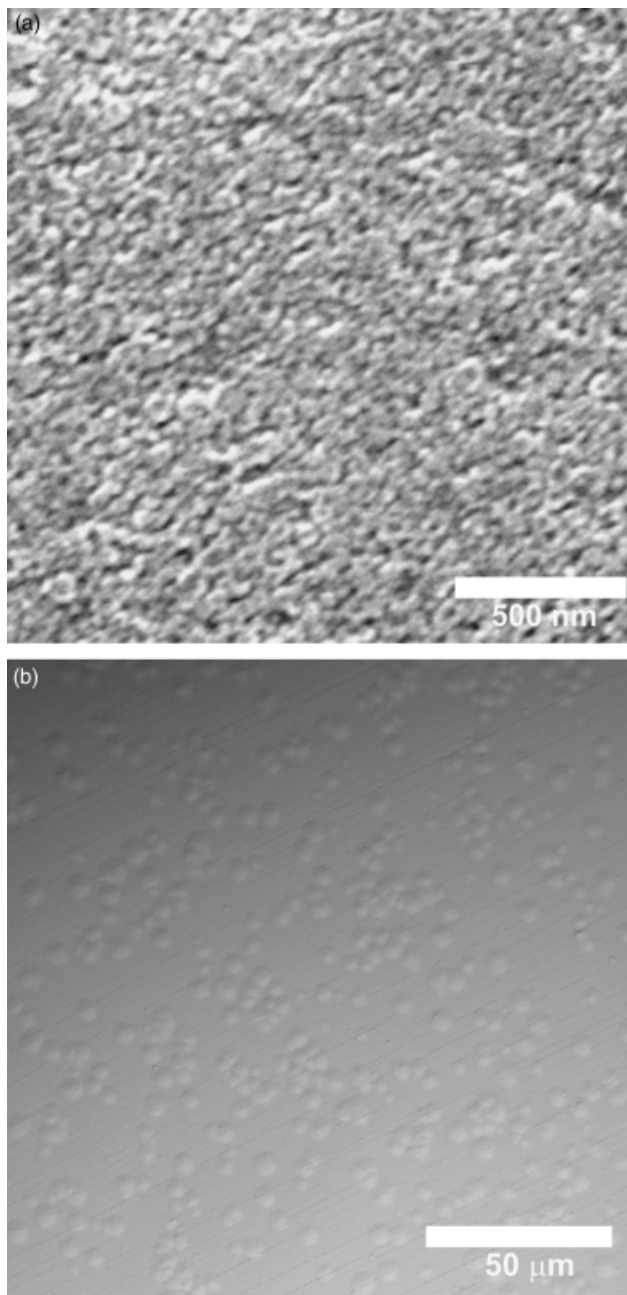


Fig. 6. (a) SEM micrograph of the fracture surface of a CERAN[®] sample etched in diluted HF solution and (b) optical microscopy of isolated crystal nucleated on the surface of a glass sample. No cracks are visible.

phase calculated for the sintered LAS glass–ceramic using Eq. (8) amounts to 219 MPa. As observed in Fig. 5, there are several microcracks in the glass particles within the microstructure. These microcracks also help to partially relieve the residual stress in the sintered glass–ceramics.

Davidge and Green²² calculated the critical diameter for spontaneous cracking around a spherical particle based on an energy balance approach. The calculations were for a circumferential crack in the matrix around the precipitate. This is not the crack configuration observed in Fig. 5(a): the precipitate (glass island) fractures along its diameter. However, the calculation for this case is very similar to those of a circumferential crack performed in Davidge and Green.²² The total energy U_T stored per unit volume in the precipitate (glass island) and in the matrix (virgilite) is $2P^2\pi R^3[(1+v_m)/2E_m + (1-2\nu_p)/E_p]$, where R is the precipitate radius²² and the subscripts m and p refer to matrix and precipitate, respectively. The energy to create a new surface U_S is $\gamma_s A$, where γ_s is the surface energy of the precip-

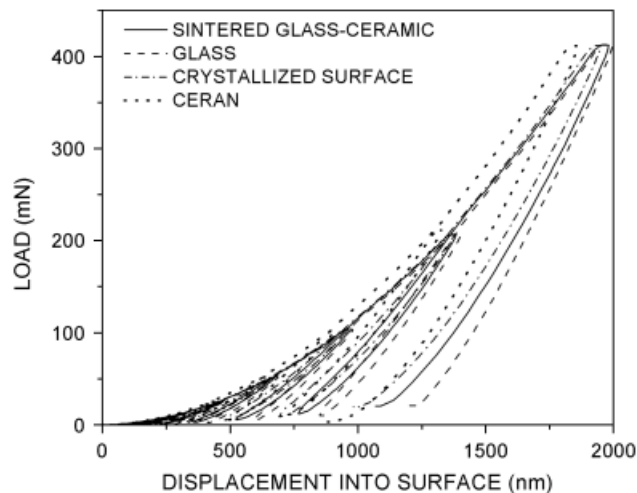


Fig. 7. Load and unloading curves for different samples.

itate and A is the area created and is $2\pi R^2$. The necessary (but not sufficient) condition for fracture is $U_T \geq U_S$. If it is assumed that 50% of U_T is spent to create the new surfaces, the critical radius for spontaneous cracking R_C will be given by:

$$R_C \geq \frac{2\gamma_s}{P^2 \left[\frac{(1+\nu_m)}{2E_m} + \frac{(1-2\nu_p)}{E_p} \right]} \quad (11)$$

We estimate the surface energy of the LAS glass as similar to that of fused silica. Assuming $\gamma_s = 4.1 \text{ J/m}^2$,^{23,24} $E_m = E_V$, $\nu_m = \nu_V$, $E_p = E_G$, $\nu_p = \nu_G$, and $P = 219 \text{ MPa}$, a critical radius

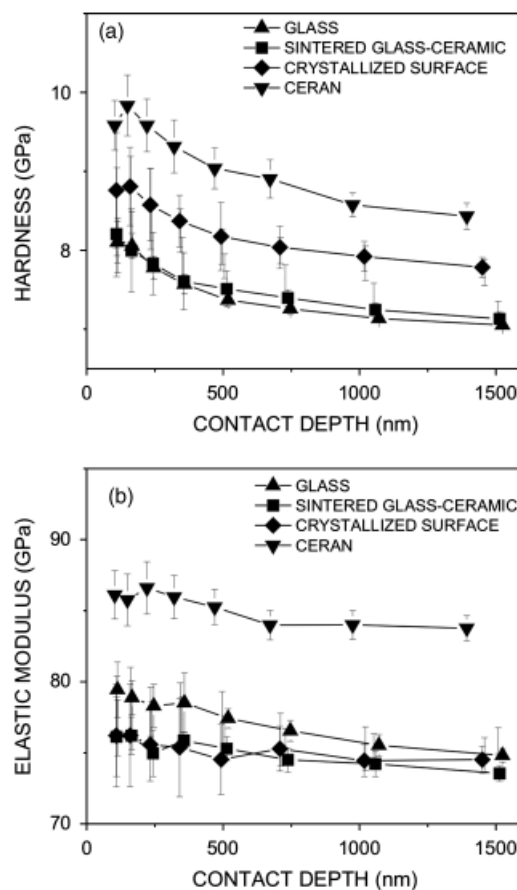


Fig. 8. (a) Hardness and (b) elastic modulus variation with contact depth for different samples.

Table III. Hardness and Elastic Modulus at Maximum Contact Depth as Measured by Instrumented Nanoindentation and Elastic Modulus and Poisson's Ratio Measured by the Pulse-Echo Technique

Sample	Instrumented indentation		Pulse-echo technique	
	H (GPa)	E (GPa)	E (GPa)	ν
Glass	7.05 (4)	74.8 (9)	75.98	0.21
Sintered glass–ceramic	7.2 (1)	74.7 (7)	81.51	0.26
Glass with crystallized surface	7.8 (1)	75 (1)		
CERAN [®]	8.4 (2)	83.8 (9)	—	—
Virgilitite	—	—	82.50*	0.27*
β -Spodumene	—	—	76.2*	0.26*

*Data calculated using a rule of mixture.

of 11 μm is obtained, which is in fair agreement with the size of cracked glass precipitates observed in Fig. 5(a). The influence of the stress fields from other precipitates, when the volume fraction is high, is neglected in this analysis. We believe that this effect is small due to the low volume fraction of glass in the sintered and CERAN[®] samples.

It should be considered that the residual stresses determined by XRD are affected by the thermal expansion anisotropy of virgilitite. In general, noncubic crystals exhibit different thermal expansion coefficients along different crystal directions. This gives rise to intergranular stresses due to the necessary accommodation of the grain volume with its neighbors. As the thermal expansion coefficients of virgilitite along its a and c crystal directions are different, the anisotropic stress state of the precipitates can be estimated using the Eshelby equivalent inclusion approach,^{25,26} considering a single thermal anisotropic spherical grain of virgilitite with two eigenstrains ϵ_1^* and ϵ_3^* in an infinite isotropic matrix of virgilitite with average properties. This is justified because the grains are randomly oriented throughout the sample. The thermal expansion of the matrix is the average thermal expansion coefficient of virgilitite $\bar{\alpha}$ given by Eq. (5), $(2\alpha_a + \alpha_c)/3$. The eigenstrains are $\epsilon_1^* = \epsilon_2^* = (\alpha_a - \bar{\alpha})\Delta T = (\alpha_a - \alpha_c)\Delta T/3$ and $\epsilon_3^* = (\alpha_c - \bar{\alpha})\Delta T = -2(\alpha_a - \alpha_c)\Delta T/3 = -2\epsilon_1^*$. The stresses are:

$$\sigma_1 = \sigma_2 = \sigma_a = -\frac{E_V(7 - 5\nu_V)}{45(1 + \nu_V)(1 - \nu_V)}\Delta\alpha\Delta T \quad (12)$$

$$\sigma_3 = \sigma_c = \frac{E_V(17 + 5\nu_V)}{45(1 + \nu_V)(1 - \nu_V)}\Delta\alpha\Delta T$$

where $\Delta\alpha = \alpha_a - \alpha_c$. Assuming the values of thermal expansion measured by XRD and assuming $\Delta T = 980^\circ\text{C}$ (the sintering temperature is 1000°C), $E_V = 82.5$ GPa, and $\nu_V = 0.27$, the intergranular stresses due to thermal anisotropy are $\sigma_a = 35$ MPa and $\sigma_c = -114$ MPa. The individual grains experience dilation along the basal plane and compression along the c -axis. This is expected because the thermal expansion is higher for the c -axis. An analysis of data presented in Table II revealed that the strains along the c -axis are much higher than those along the a -axis for the sintered and CERAN[®] samples, which is in qualitative agreement with the theoretical predictions given by Eq. (12). We expect the real effect of thermal expansion anisotropy of virgilitite to be smaller than calculated here because the crystals are partially embedded in residual glass as shown in Fig. 5(c). The average intergranular stress is $(2\sigma_a + \sigma_c)/3 = -15$ MPa.

The thermal expansion anisotropy of virgilitite may induce grain-boundary microcracking. This has been observed for magnesium and aluminum titanate ceramics. Evidences of grain-boundary microcracking during cooling are provided by the reduction in the apparent thermal expansion, events of acoustic emission, and thermal expansion hysteresis.^{27–30} Indeed, Fig. 4

shows for the sintered glass–ceramics and the commercial CERAN[®] the occurrence of thermal expansion hysteresis, which increases with the number of cycles. Also, the average thermal expansion of virgilitite estimated by dilatometry is different from that measured by XRD. The critical grain size D_g above which intergranular cracking is observed is the following equation³¹:

$$D_g = \frac{5.2(1 + \nu_V)^2\gamma_{GB}}{E_V(\Delta\alpha\Delta T)^2} \quad (13)$$

where γ_{GB} is the grain-boundary surface energy and $\Delta\alpha$ is half of the maximum difference in thermal expansion due to anisotropy. Assuming the surface energy γ_{GB} the same as for the glass, $\Delta T = 980^\circ\text{C}$, $E_V = 82.5$ GPa, $\nu_V = 0.27$, and $\Delta\alpha = -1.6 \times 10^{-6} \text{ }^\circ\text{C}^{-1}$, a critical grain size of 170 μm is estimated. This is a very large grain size in comparison with the investigated microstructures, and as a result, grain-boundary microcracking is an unlikely phenomenon in sintered LAS glass–ceramic and CERAN[®].

Figure 5(c) shows that in a scale of a few micrometers there is some residual glass around the crystals. This residual glass is under tension and thus there should be a critical radius of the virgilitite precipitate for radial cracking in the glass. We estimate the critical size using a model proposed by Todd and Derby²⁶—which is based on Green's model³² for radial microcracking around an isolated precipitate and incorporates the effect of a finite volume fraction of precipitates. This model considers a spherical shell of matrix (glass) with radius b around a spherical precipitate (virgilitite) with radius R . The radius b is related to the volume fraction f of virgilitite precipitates as $b = R/f^{1/3}$. An annular crack of length a growing around the virgilitite precipitate is approximated by a circular crack with the tangential stress in the matrix, σ_t , originated by the thermal expansion mismatch between particle and matrix acting on its faces, i.e. $R < r < R + a$, as shown in Fig. 9. The resultant stress intensity factor is:

$$K = \frac{P\sqrt{a(a+2R)}(R^2 + 2f(a+R)^2)}{\sqrt{\pi}(1-f)(a+R)^{3/2}} \quad (14)$$

where K is maximum when the total crack length is from the precipitate up to the outer boundary of the matrix shell, i.e. a is equal to $b - R$. Therefore, assuming the condition for microcracking ($K = K_{IC}$) when $a = b - R$, the rearrangement of Eq. (13) yields an expression for the critical radius R_c of the virgilitite precipitate for spontaneous microcracking:

$$R_c = \frac{\pi(1-f)^2}{f(1-f^{2/3})(1+2f^{1/3})^2} \left(\frac{K_{IC}}{P}\right)^2 \quad (15)$$

Assuming $K_{IC} = 0.7 \text{ MPa} \cdot \text{m}^{1/2}$,³³ $f = 0.89$, and $P = -35$ MPa, the critical radius is 27 μm for the sintered glass–ceramic. For CERAN[®], a similar calculation yields a critical radius of 19 μm . These values are considerably greater than the observed

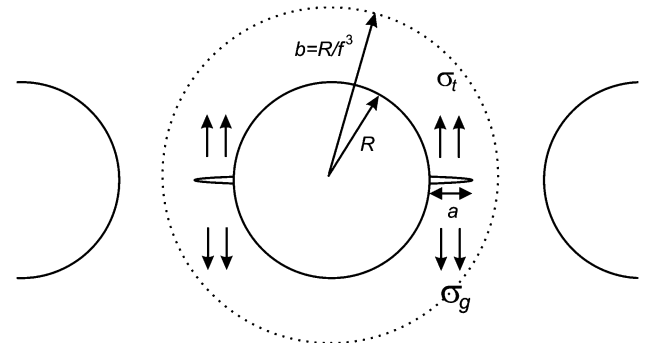


Fig. 9. Annular crack configuration in the glass residual phase growing radially from the crystal with radius R (adapted from Mura²⁵).

crystal diameters in the respective microstructures. Thus, microcracking appears to be unlikely in the residual glass phase around the crystalline particles.

V. Conclusions

Internal residual stress analyses by Synchrotron XRD in two types of LAS glass–ceramics led to several findings. First, the average residual stresses in the virgilite crystals in the sintered LAS glass–ceramic and CERAN[®] were only -34 MPa (compressive) and -87 MPa, respectively. These experimental values are close to the theoretically predicted stresses if the high volume fraction of the crystalline phase in these glass–ceramics is considered. On the other hand, residual stresses in experimental glass–ceramics having $5\ \mu\text{m}$ individual crystals on the surface or a $15\ \mu\text{m}$ crystallized layer were approximately -250 and -380 MPa, respectively. These high values are similar to those theoretically predicted by the Selsing model and for the case of a thin film on a substrate with different thermal expansion coefficient.

Microcracking of the largest glass islands was observed in the sintered glass–ceramic. Using a modified Green model, the calculated critical (glass) island diameter for fracture was in good agreement with experimental observations. Because of the thermal expansion anisotropy of virgilite, the lattice strains are highly anisotropic. The experimental data allowed the calculation of the critical crystal diameters for grain-boundary microcracking due to the anisotropy of thermal expansion of virgilite, and for microcracking in the residual glass phase surrounding the virgilite particles. These parameters are important for the successful design of sintered glass–ceramics.

Acknowledgment

The authors acknowledge Prof. Carlos M. Lepienski for the use of the Nanoindenter XP and Prof. Carlos Paiva-Santos for very fruitful discussions on Riveteld refinement of XRD data.

References

- ¹ a) P. W. McMillan, *Glass–Ceramics*, 2nd edition, Academic Press Inc., New York, USA, 1979. b) W. Höland, G. Beall, *Glass–Ceramic Technology*. The American Ceramic Society, Ohio, USA, 2002.
- ² E. D. Zanotto, “A Bright Future to Glass–Ceramics,” *Am. Ceram. Soc. Bull.*, **89**[8], 19–27 (2010).
- ³ V. R. Mastelaro and E. D. Zanotto, “Residual Stresses in a Soda-Lime-Silica Glass–Ceramic,” *J. Non-Cryst. Solids*, **194**, 297–304 (1996).
- ⁴ V. R. Mastelaro and E. D. Zanotto, “Anisotropic Residual Stresses in Partially Crystallized $\text{Li}_2\text{O}-2\text{SiO}_2$ Glass–Ceramics,” *J. Non-Cryst. Solids*, **247**, 79–86 (1999).
- ⁵ H. Pinto, L. Ito, M. Crovace, E. B. Ferreira, F. Fauth, T. Wroblewski, E. D. Zanotto, and A. R. Pyzalla, “Surface and Bulk Residual Stresses in $\text{Li}_2\text{O} \cdot 2\text{SiO}_2$ Glass–Ceramics,” *J. Non-Cryst. Solids*, **353**, 2307–1 (2007).
- ⁶ J. W. Zwanziger, U. Werner-Zwanziger, E. D. Zanotto, E. Rotari, L. N. Glebova, L. B. Glebov, and J. F. Schneider, “Residual Internal Stress in

Partially Crystallized Photo Thermo Refractive Glass: Evaluation by Nuclear Magnetic Resonance Spectroscopy and First Principles Calculations,” *J. Appl. Phys.*, **99**, 083511, 6pp (2006).

⁷ G. Müller, “Structure, Composition, Stability and Thermal Expansion of High-Quartz and Keatite Type Alumino-Silicates”; pp. 13–25 in *Low Thermal Expansion Glass Ceramics*, Edited by H. Bach. Springer-Verlag, Berlin, 1995.

⁸ R. Muller, E. D. Zanotto, and V. M. Fokin, “Surface Crystallization of Silicate Glasses: Nucleation Sites and Kinetics,” *J. Non-Cryst. Solids*, **274**, 208–31 (2000).

⁹ S. Knickerbocker, M. R. Tuzzolo, and S. Lawhorne, “Sinterable β -Spodumene Glass–Ceramics,” *J. Am. Ceram. Soc.*, **72**, 1873–9 (1989).

¹⁰ A. C. Larson and R. B. Von Dreele, “General Structure Analysis System (GSAS); Report LAUR 86-748, Los Alamos National Laboratory, 2004.

¹¹ B. H. Toby, “EXPGUI, A Graphical User Interface for GSAS,” *J. Appl. Cryst.*, **34**, 210–3 (2001).

¹² M. H. Sadd, *Elasticity, Theory, Applications and Numerics*, 1st edition, Elsevier Inc., Amsterdam, 2005, p. 74.

¹³ W. C. Oliver and G. M. Pharr, “An Improved Technique for Determining Hardness and Elastic Modulus Using Load and Displacement Sensing Indentation Experiments,” *J. Mater. Res.*, **7**, 1564–83 (1992).

¹⁴ J. Selsing, “Internal Stresses in Ceramics,” *J. Am. Ceram. Soc.*, **44**, 419 (1961).

¹⁵ M. Ohring, *The Materials Science of Thin Films*. Academic Press, New York, 1991.

¹⁶ C.-H. Hsueh and P. F. Becher, “Residual Thermal Stresses in Ceramic Composites. Part I: With Ellipsoidal Inclusions,” *Mater. Sci. Eng.*, **A212**, 22–8 (1996).

¹⁷ R. D. Mindlin and D. H. Cheng, “Thermoelastic Stress in the Semi-Infinite Solid,” *J. Appl. Phys.*, **21**, 931–3 (1950).

¹⁸ V. M. Hauk and E. Macherauch, “A Useful Guide for X-Ray Stress Evaluation (XSE),” *Adv. X-Ray Anal.*, **27**, 81–99 (1983).

¹⁹ I. Levin, W. D. Kaplan, and D. G. Brandon, “Residual Stresses in Alumina-SiC Nanocomposites,” *Acta Metall.*, **42**, 1147–54 (1994).

²⁰ O. Peitl, F. C. Serbena, V. R. Mastelaro, and E. D. Zanotto, “Internal Residual Stress Measurements in a Bioactive Glass–Ceramic Using Vickers Indentation,” *J. Am. Ceram. Soc.*, **93**, 2359–68 (2010).

²¹ R. W. Davidge, *Mechanical Behaviour of Ceramics*, 1st edition, Cambridge University Press, Cambridge, 1979, p. 120.

²² R. W. Davidge and T. J. Green, “The Strength of Two-Phase Ceramic/Glass Materials,” *J. Mater. Sci.*, **3**, 629–34 (1968).

²³ J. P. Lucas, “Determining Fracture Toughness of Vitreous Silica Glass,” *Ser. Metall.*, **32**, 743–8 (1995).

²⁴ B. D. Beake and J. F. Smith, “High-Temperature Nanoindentation Testing of Fused Silica and Other Materials,” *Philos. Mag. A*, **82**, 2179–86 (2002).

²⁵ T. Mura, *Micromechanics of Defects in Solids*. Martinus Nijhoff, Dordrecht, 1987.

²⁶ R. I. Todd and B. Derby, “Thermal Stress Induced Microcracking in Alumina–20% SiCp Composites,” *Acta Mater.*, **52**, 1621–9 (2004).

²⁷ J. A. Kuszyk and R. C. Bradt, “Influence of Grain Size on Effects of Thermal Expansion Anisotropy in MgTi_2O_7 ,” *J. Am. Ceram. Soc.*, **56**, 420–3 (1973).

²⁸ Y. Ohya and Z. Nakagawa, “Grain-Boundary Microcracking Due to Thermal Expansion Anisotropy in Aluminum Titanate Ceramics,” *J. Am. Ceram. Soc.*, **70**, C184–6 (1987).

²⁹ F. J. Parker and R. W. Rice, “Correlation Between Grain Size and Thermal Expansion for Aluminum Titanate Materials,” *J. Am. Ceram. Soc.*, **72**, 2364–6 (1989).

³⁰ Y. Ohya and Z. Nakagawa, “Measurement of Crack Volume Due to Thermal Expansion Anisotropy in Aluminium Titanate Ceramics,” *J. Mater. Sci.*, **31**, 1555–9 (1996).

³¹ A. G. Evans, “Microfracture from Thermal Expansion Anisotropy—I. Single Phase Systems,” *Acta Metall.*, **26**, 1845–53 (1978).

³² D. Green, “Stress Induced Microcracking at Second Phase Inclusions,” *J. Am. Ceram. Soc.*, **64**, 138–41 (1981).

³³ P. Vullo and M. J. Davis, “Comparative Study of Micro-Indentation and Chevron Notch Fracture Toughness Measurements of Silicate and Phosphate Glasses,” *J. of Non-Cryst. Solids*, **349**, 180–4 (2004). □